Steel and Composite Structures, *Vol. 21, No. 3 (2016) 605-628*
DOI: http://dx.doi.org/10.12989/scs.2016.21.3.605

Energy absorption characteristics of diamond core columns under axial crushing loads

Nader Vahdat Azad and Saeed Ebrahimi*

Mechanical Engineering Department, *Yazd University*, *Yazd*, *Iran*

(*Received August 04, 2015, Revised February 11, 2016, Accepted May 14, 2016*)

Abstract. The energy absorption characteristics of diamond core sandwich cylindrical columns under axial crushing process depend greatly on the amount of material which participates in the plastic deformation. Both the single-objective and multi-objective optimizations are performed for columns under axial crushing load with core thickness and helix pitch of the honeycomb core as design variables. Models are optimized by multi-objective particle swarm optimization (MOPSO) algorithm to achieve maximum specific energy absorption (SEA) capacity and minimum peak crushing force (PCF). Results show that optimization improves the energy absorption characteristics with constrained and unconstrained peak crashing load. Also, it is concluded that the aluminum tube has a better energy absorption capability rather than steel tube at a certain peak crushing force. The results justify that the interaction effects between the honeycomb and column walls greatly improve the energy absorption efficiency. A ranking technique for order preference (TOPSIS) is then used to sort the non-dominated solutions by the preference of decision makers. That is, a multi-criteria decision which consists of MOPSO and TOPSIS is presented to find out a compromise solution for decision makers. Furthermore, local and global sensitivity analyses are performed to assess the effect of design variable values on the SEA and PCF functions in design domain. Based on the sensitivity analysis results, it is concluded that for both models, the helix pitch of the honeycomb core has greater effect on the sensitivity of SEA, while, the core thickness has greater effect on the sensitivity of PCF.

Keywords: diamond core; honeycomb columns; optimization; sensitivity analysis; crashworthiness; energy absorption; response surface method

1. Introduction

In the crashworthiness analysis of engineering applications such as vehicle engineering, shipbuilding, civil engineering and other industries, the energy absorption characteristics of the honeycomb sandwich columns have found great attention. The demanded level of safety in such applications is achieved by maximizing the specific energy absorption capacity and minimizing the peak crushing force. This important issue is treated by absorbing the initial kinetic energy during impact, keeping the force levels adequately low and passing damage to the system.

One of the most important applications of the energy absorbers can be addressed in automotive engineering. Different criteria are being used to assess crashworthiness, including the deformation

*Corresponding author, Associate Professor, E-mail: ebrahimi@yazd.ac.ir
[a] Ph.D. Candidate, E-mail: nader.vahdat@yahoo.com

http://www.techno-press.org/?journal=scs&subpage=6 ISSN: 1229-9367 (Print), 1598-6233 (Online)

shape of car structure, the acceleration experienced by the vehicle during an impact, and the possibility of hurt predicted by human body models. When designing an energy absorber for a structure like a car, different factors such as the energy absorption per unit mass, the maximum crushing force, etc., can be used to evaluate its performance. Reduction of mass and increasing safety are usually desired in the design of energy absorbing elements of a car. Therefore, higher specific energy absorption (SEA) is often considered as an important factor in this context.

A chief contest remains how to seek an optimal structure for the energy absorbing components such that the highest crashworthiness efficiency can be achieved. An optimization problem contains high nonlinearities of material and shape, which have not been effectively addressed except some empirical closed form solutions or surrogate model techniques were adopted (Yang *et al*. 2005, Wang and Shan 2007, Lu and Yu 2003). Abramowicz and Jones (1984a, b) made static and dynamic experiments on square and circular steel cylinders and compared the outcomes with conceptual computation.

The Response Surface Method (RSM) has been widely used to solve complicated design optimization issues including contact, material and geometrical nonlinearities. The RSM and its applications in crashworthiness design have been utilized by a large number of researchers, e.g., Lee *et al*. (2002), Chiandussi and Avalle (2002), Avalle *et al*. (2002), Kim (2002), and Lanzi *et al*. (2004). Lanzi *et al*. (2004) applied radial basis functions (RBF) to the optimal shape design of composite absorbers. Fang *et al*. (2005) also used RBF to achieve crashworthiness optimization using a vehicle model. Kodiyalam *et al*. (2004) studied multidisciplinary design of vehicles based on approximation models by the Kriging method.

Multi-objective optimization, as a more practical design methodology, directs at addressing a number of design principles, which has become an attractive research topic in crashworthiness design lately (Zarei and Kroger 2006, Sinha 2007). A multi-objective optimization procedure normally generates a group of solutions in a Pareto sense. As such, a more insight of the optimal design space may be provided to allow creation of a better design result (Liao *et al*. 2007).

Acar *et al*. (2011) performed multi-objective crashworthiness optimization of tapered circular thin-walled tubes with axisymmetric indentations for maximum crush force efficiency and maximum SEA. Sun *et al*. (2010a) first used the particle swarm optimization (PSO) in honeycomb crashworthiness design based on a two-stage multi-fidelity method for surrogate models. The multi-objective particle swarm optimization (MOPSO) algorithm was also adopted by Sun *et al*. (2010b) to seek optimal crashworthiness designs for functionally graded foam (FGF) structures. Multicriteria design is formulated as both constrained single-objective and multiple-objective optimization problems for thin-walled aluminum structures, where cross sectional sizes of single-, double-, triple- and quadruple-cell columns were taken (Hou *et al*. 2008). Yin *et al*. (2014) analyzed foam-filled multi-cell thin-walled structure (FMTS) to achieve the most excellent crashworthiness characteristics. A robust design methodology was used to investigate the effects of parametric uncertainties of foam-filled thin-walled structures on the design optimization (Sun *et al*. 2014). Their approach is well-suited to overcome the less-meaningful or even unacceptable results of conventional deterministic optimization approaches when considering the perturbations of design variables and noises of system parameters. Yin *et al*. (2011) investigated the energy absorption characteristics of honeycomb-filled single and bi-tubular polygonal tubes (HSBPT). They adopted multi-objective optimization algorithm to achieve maximum SEA capacity and minimum PCF. Energy absorption properties of metal square honeycombs and size optimization were studied by Li *et al*. (2014). The preprocessing software Patran was used to build FE models, and the explicit solver LSDYNA was employed to perform the crashworthiness analyses.

The preconception to increase the plastic deformation zones of thin-walled columns through buckling of different honeycomb sandwich lattices is based on the fact that more tube walls are folded locally. This interaction strengthening effect between honeycomb core and tubes is used to improve the crush resistant force and increase the energy absorption. The use of lightweight materials as honeycomb cores affects the bending mode of thin-walled hollow cylinder, shortens bending lengths and increases number of lobes. Furthermore, the interaction effects due to the multi-axial compression of the filling cores increase the energy absorption of the filling thin-walled columns. However, in the compressed foam-filled tubes, a considerable amount of material does not participate in the plastic deformation which in turn reduces the energy absorption efficiency of the column (Zhang *et al*. 2010 and 2011).

The present study aims at maximizing the SEA and minimizing the PCF for thin-walled diamond core honeycomb cylindrical structures in an explicit finite element framework. By means of numerical simulation methods, the crashworthiness of sandwich column under axial crushing loads is inspected. Models are optimized by multi-objective particle swarm optimization algorithm to achieve maximum SEA capacity and PCF. Furthermore, a local and global sensitivity analysis is performed to assess the effect of design variable values on the SEA and PCF functions in design domain. Depending on the fields of application, different definitions can be encountered, see e.g., Saltelli *et al*. (2006).

2. Theory

2.1 Response surface method

In the multi-objective optimization of crashworthiness, mathematical formulation of the objective functions including crushing force and energy absorption is required. Analytical formulation of these functions with respect to shape and material parameters may be very difficult. In general, substantial data are usually obtained for constructing empirical formulae of these relationships through experimental studies. The RSM has been presented by Myers and Montgomery (2002) and has been extensively used by other researchers e.g., Oktem *et al*. 2005. This approach uses some simple basic functions such as polynomials to approximate the crash behaviour of a structure. This method has been applied to optimize thin-walled structures with crashworthiness criterion (Hou *et al*. 2007, Xiang *et al*. 2006).

However, as a typical alternative modeling technique, RSM (Jansson *et al*. 2003) has been widely used for solving complicated design optimization problems including contact, material and geometrical nonlinearities. The concept is to express a complex function $y(x)$ in terms of a series of simple basis functions $\beta_j(x)$, as

$$y(x) = \tilde{y}(x) + e = \sum_{j=1}^{n} a_j \, \beta_j(x) + e \tag{1}$$

where $\tilde{y}(x)$ denotes the approximation function of the real response $y(x)$ (including crushing force and energy absorption functions) and e denotes the error (Lee and Lee 2005, Forsberg and Nilsson 2005 and 2006). Usually, polynomial functions are selected as the basis functions for its simplicity. Selection of the type of polynomial functions depends on the required order as well as number of sampling points for which the best fitting process can be followed. The unknowns $a_j\,(j = 1, \ldots, n)$ are determined based on the m sampling points $x_i\,(j = 1, \ldots, m, m > n)$ (Hou S

et al. 2009). For generating a response vector $y = (y_1, \dots, y_m)^T$, the finite element analysis is performed for each sample point. The unknown vector $a = (a_1, \dots, a_m)^T$ is then determined via the least squares of the deviation between the response vector y and the approximated function $\tilde{y}$ at all sampling points, as

$$E(a) = \sum_{i=1}^{m} e_i^2 = \sum_{i=1}^{m} (y_i - \tilde{y}_i)^2 = \sum_{i=1}^{m} (y_i - \sum_{j=1}^{n} (a_j \beta_j (x_i)))^2 \tag{2}$$

This leads to the linear system of equations in the form of

$$\begin{pmatrix} y_1 \\ \vdots \\ y_m \end{pmatrix} = \begin{bmatrix} \beta_1(x_1) & \dots & \beta_n(x_n) \\ \vdots & \ddots & \vdots \\ \beta_1(x_m) & \dots & \beta_m(x_m) \end{bmatrix} \begin{pmatrix} a_1 \\ \vdots \\ a_n \end{pmatrix} \rightarrow \; y = \beta a \tag{3}$$

Solving this system of equations leads to the following result

$$a = (\beta^T \beta)^{-1} \beta^T y \tag{4}$$

Metamodels are widely used in the optimization problems. In the following study, metamodels of the objective functions are constructed by applying polynomial functions. Based on these developed metamodels, we can compute the corresponding objective function values of any design variable in the design space. In this study, the multi-objective particle swarm optimization (MOPSO) algorithm is utilized to create the Pareto front of the two conflicting objectives of SEA and PCF. The Pareto front can supply the designer with a domain of optimal solutions for their further decision making. The MOPSO is a population based optimization approach, first developed by Kennedy and Eberhart (1995) and has found significant attention lately due to its comparatively fast convergence and well-distributed Pareto front, compared with other multi-objective optimization algorithms. The PSO shares many similarities with evolutionary computation techniques such as Genetic Algorithms (GA). In the PSO, the potential solutions, called particles, fly through the problem space by following the current optimum particles.

In order to evaluate the accuracies of the developed metamodels, the relative error (RE) between the FEA result $y(x)$ and $\tilde{y}(x)$ is calculated as

$$RE = \frac{y(x) - \tilde{y}(x)}{y(x)} \tag{5}$$

The accuracies of these metamodels can be evaluated based on the root mean square error (RMSE), the maximum absolute error (MAX) and *R* square value, which are written respectively as

$$RMSE = \sqrt{\frac{SSE}{k}} \tag{6}$$

$$MAX = \max|y_i - \tilde{y}_i|, \quad i = 1,2, \dots, k \tag{7}$$

$$R^2 = 1 - \frac{SSE}{SST}, \tag{8}$$

where k is the number of design points. The smaller the values of $RMSE$ and MAX, or the larger the value of R^2, the more accurate the metamodel. The variable $RMSE$ is used to measure the overall accuracy of the model, while MAX is used to gauge the local accuracy of the model. Parameters SSE and SST are sum of the squared errors and total sum of squares in the following forms, respectively

$$SSE = \sum_{i=1}^{k} (y_i - \tilde{y}_i)^2, \tag{9}$$

$$SST = \sum_{i=1}^{k} (y_i - \bar{y})^2, \tag{10}$$

where $\bar{y}$ is the mean value of y_i.

2.2 Crashworthiness

The study on the crashworthiness of thin-walled structures and optimization of their performance is usually started from the definition of the crashworthiness indicator. The force displacement curves of a typical thin-walled structure, as demonstrated in Fig. 1, can measure the impact characteristics to a certain extent. The absorbed energy E is equivalent to the mechanical work done by the impact force during the crush distance d (Fig. 1) and therefore, is calculated as

$$E(d) = \int_0^d F(x)dx \tag{11}$$

The average force (F_{avg}) for a given deformation can be calculated as

$$F_{avg} = \frac{E(d)}{d} \tag{12}$$

To specifically define the energy absorption capabilities of different materials and weights, the specific energy absorbed per unit mass M is defined by

$$SEA = \frac{E}{M} \tag{13}$$

Obviously, a higher SEA value indicates a higher capability of energy absorption capability.

As it is basically very difficult to measure the crashworthiness in terms of a unique physical quantity or mathematical formula, the crashworthiness optimization is consequently served to seek the best possible design of structure for a desirable crashing performance. Before to proceed to the main part of the article, some preliminary materials are briefly discussed in the next sections to establish the required background.

2.3 Optimization

Multi-objective optimization, which is also known as multicriteria optimization or vector optimization, is generally defined as finding a vector of design parameters satisfying constraints to

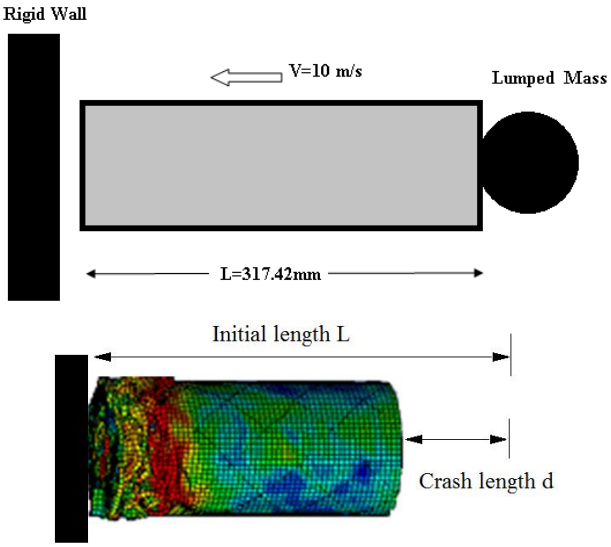

Fig. 1 The impact model with lumped Mass

give satisfactory values to all objective functions. In such problems, there are a number of objectives or cost functions to be optimized (minimized or maximized) simultaneously. These objectives may conflict with each other so that improving one of them will deteriorate another. As a result, no single optimal solution can be found as the best with respect to all of the objective functions. In such case, a set of optimal solutions, known as Pareto optimal solutions or Pareto front is to be found for multi-objective optimization problems. These optimal solutions are non-dominated to each other and could not lead to the improvement of all objectives simultaneously but are superior to the rest of solutions in the search space (Ebrahimi S and Vahdat azad N 2015).

2.4 MCDM Method

Decision-making problem is the process of finding the best option from all of the feasible alternatives. In almost all such problems, the multiplicity of criteria for judging the alternatives is pervasive. That is, for many such problems, the decision maker wants to solve a multiple criteria decision making (MCDM) problem. In classical MCDM methods, the ratings and the weights of the criteria are known precisely. In this paper, a ranking process called TOPSIS (technique for order preference by similarity to an ideal solution) is used for solving this kind of MCDM problem in order to rank the solutions in Pareto frontier and choose the best possible compromise. TOPSIS is based on the concept that the best alternative should have the shortest distance from the positive-ideal solution and the longest distance from the negative-ideal solution (Hwang and Yoon 1981). The reasons of using TOPSIS are the concept behind TOPSIS which is rational and comprehensible, and the computation involved is simple (Deng *et al*. 2000). The TOPSIS method is expressed in a succession of six steps as follows:

Step 1: Calculate the normalized decision matrix. The decision matrix collects *m* alternatives for *n* attributes (criteria). The normalized value r_{ij} is calculated from the components x_{ij} of the decision matrix as follows

$$r_{ij} = x_{ij} / \sqrt{\sum_{i=1}^{m} x_{ij}^2} \qquad i = 1, 2, ..., m \quad \text{and} \quad j = 1, 2, ..., n. \tag{14}$$

Step 2: Calculate the weighted normalized decision matrix. The weighted normalized value v_{ij} is calculated as follows

$$v_{ij} = r_{ij} \times w_{ij} \qquad i = 1, 2, ..., m \text{ and } j = 1, 2, ..., n. \tag{15}$$

where w_{ij} is the weight of the j^{th} criterion or attribute and $\sum_{j=1}^{n} w_j = 1$. In this study, the weights are determined using the entropy method (Lin C.T *et al* 2006).

Step 3: Determine the ideal (A^*) and the negative ideal (A^-) solutions.

$$A^* = \{(max_i\, v_{ij} \,|j \in C_b), (min_i\, v_{ij} \,|j \in C_c)\} = \{v_j^* \,|\, j = 1,2, \dots, m\} \tag{16}$$

$$A^- = \{(min_i\, v_{ij} \,|j \in C_b), (max_i\, v_{ij} \,|j \in C_c)\} = \{v_j^- \,|\, j = 1,2, \dots, m\} \tag{17}$$

Step 4: Calculate the separation measures using the *m*-dimensional Euclidean distance. The separation measures of each alternative from the positive ideal solution and the negative ideal solution, respectively, are as follows

$$S_i^* = \sqrt{\sum_{j=1}^{m} (v_{ij} - v_j^*)^2}, j = 1,2, \dots, m \tag{18}$$

$$S_i^- = \sqrt{\sum_{j=1}^{m} (v_{ij} - v_j^-)^2}, j = 1,2, \dots, m \tag{19}$$

Step 5: Calculate the relative closeness to the ideal solution. The relative closeness of the alternative A_i with respect to A^* is defined as follows:

$$RC_i^* = \frac{S_i^-}{S_i^* + S_i^-}, i = 1,2, \dots, m \tag{20}$$

Step 6: Rank the preference order. As a result, this method is considered to be able to acquire a satisfactory compromise solution for a MCDM problem (Chen and Tzeng 2004). MCDM model, which integrates the techniques of order preference by similarity to ideal solution (TOPSIS) with gray relation analysis (GRA), is implemented to find a best compromise optimum from the Pareto set (Fang *et al*. 2015).

2.5 Sensitivity analysis

Sensitivity analysis is the complementary tool used to study how the uncertainty in the model output can be apportioned to different sources of uncertainty. In the sensitivity analysis, it is basically intended to investigate how any uncertainty in the system output can be related to

different sources of uncertainty in its inputs (Saltelli *et al*. 2008). Sensitivity analysis methods can be classified as either local or global.

2.5.1 Local sensitivity

Local sensitivity analysis falls generally in the class of the so-called One-A-Time method, as each factor is perturbed in turn while keeping all other factors fixed at their nominal value. In the present study, this normalized sensitivity formulation is used to assess the effect of design variable values on the specific energy absorption and peak crushing force function in design domain.

2.5.2 Global sensitivity

Global sensitivity analysis studies the effect of input variations on the outputs in the entire allowable ranges of the input space. Global sensitivity analysis methods are variance-based methods which use variance as an indicator of the importance of an input parameter and consequently, rely closely on sampling methods and input parameter distribution. The importance of the given input parameter can be measured by a term defined as the sensitivity measure, which is often defined as the fractional contribution to the output variance due to uncertainties in the inputs. In this context, the Method of Sobol uses decomposition of variance to calculate the so-called Sobol's sensitivity indices. Using combinations of input parameters in increasing dimensionality, the model output function $y = f(x)$ is basically decomposed into summands of variance. This method is one of the most established and widely used methods which is capable of computing the Total Sensitivity Indices (TSI). Based on the TSI, the main effects of a given parameter and all the interactions (of any order) involving that parameter can be measured (Ebrahimi and Vahdatazad 2015).

2.6 Finite element model

Diamond core types of honeycomb sandwich columns are investigated numerically by ABAQUS, which are aluminium core with two different materials in inner and outer tubes containing steel and aluminium, as shown in Fig. 2. The length (L) of the column is 317.42 mm. The inner and outer radiuses (R_i, R_o) of the circular tubes are 30 and 50 mm, respectively. The wall thickness of core t is the first design variable. The pitch of the honeycomb core (as shown in Fig. 3) that is defined in Eq. (21) is the second design variable.

$$K = \frac{\text{core pitch}}{\text{length (L) of the column}} \tag{21}$$

Fig. 3 illustrates definition of the honeycomb core pitch. Based on this figure, it is seen that the core pitch is the length of that part of column for which one cycle of the diamond honeycomb core is created.

In addition, it is noticeable that according to Eq. (21), parameter K is actually obtained from the distance between the start and end points of one pitch divided by the column length. In other words, for example, for K = 2 the distance between the start and end points of one column pitch extrude would be twice of the column length, and so on.

The cell number of honeycomb sandwich columns in circumferential direction is six. In this paper, two models are investigated: the first model contains two steel cylindrical tubes with aluminium core and the second model contains two aluminium cylindrical tubes with aluminium core that are listed in Table 1. Four-node quadrilateral shell elements were created. Contact was

Outer and inner tubes Diamond honeycomb Sandwich column

Fig. 2 Geometrical configuration of sandwich column

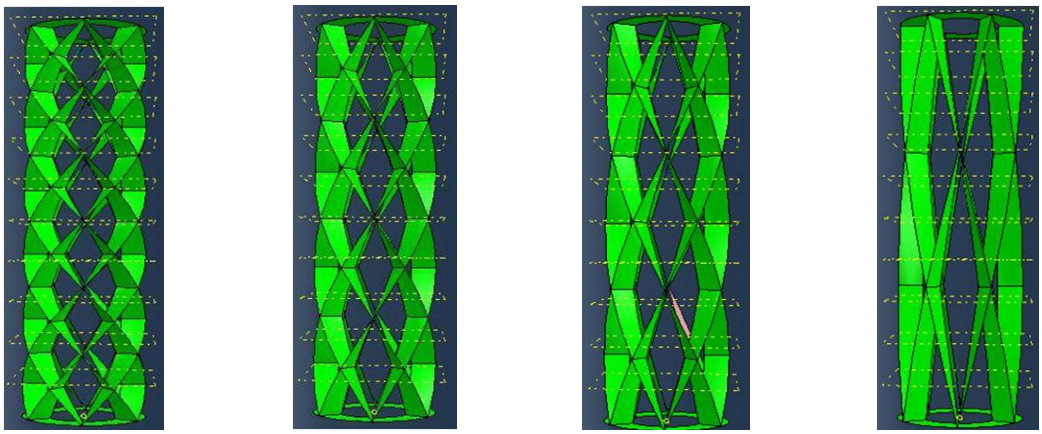

Pitch of helix = L
K = 1

Pitch of helix = 1.5 L
K = 1.5

Pitch of helix = 2 L
K = 2

Pitch of helix = 4 L
K = 4

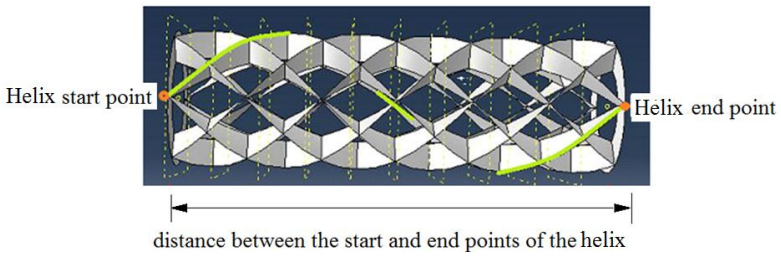

Fig. 3 Definition of honeycomb core pitch K

defined between the rigid wall and the top of the cylinder by creating surfaces in ABAQUS. The contact between the rigid body and the specimen is modelled with a node-to-surface contact with the dynamic and static friction coefficient of 0.2.

Table 1 Properties of the honeycomb columns

Model	Material properties			Inner and outer tube thickness (mm)
	Inner tube	Outer tube	Core	
Steel tube	Mild steel	Mild steel	Aluminum alloy	0.4
Aluminum tube	Aluminum alloy	Aluminum alloy	Aluminum alloy	1

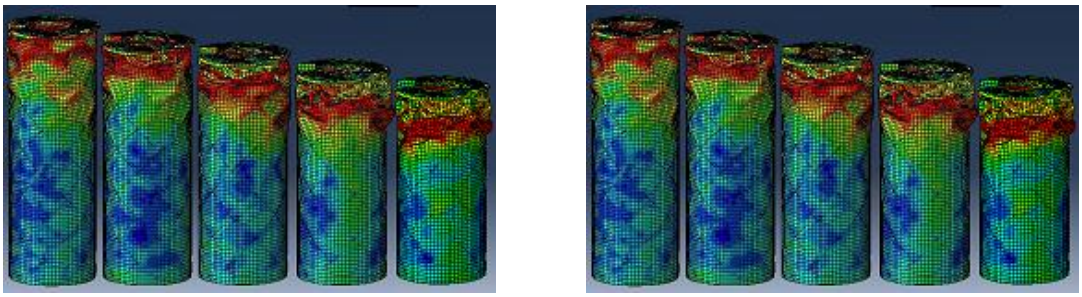

Fig. 4 Deformation profiles of the diamond honeycomb sandwich column

The full sections are modeled using the quadrilateral Belytschko-Tsay four-node shell element and five integration points are used throughout the thickness. The total number of elements used for FEA is 26000. Prescribed velocity 10 m/s is applied to the honeycomb sandwich column and lumped mass to crush the rigid wall. The analysis time is set to 0.01 s, which is enough for presenting an entire force curve. To more clearly show the energy absorption behavior, an extra lumped mass of 500 kg was attached to the free end of the column. FEM simulations of axial crushing were performed and a successive folding pattern was formed as shown in Fig. 4. Some cutting views of the deformation profiles of the square sandwich column are also shown in Fig. 4.

2.7 Material properties

Aluminum and its alloys signify one class of favorable energy-absorbing materials due to their relative high ratio of functionality to weight, which have been widely adopted in the structural design of vehicles. Aluminum is of very good formability and almost any realistically shaped multiply-connected cross-sectional can be produced by an extrusion process, which provides a considerable possibility to economically implement a specific design of sectional configuration. Aluminum becomes more and more important to optimize the sectional parameters to achieve the best possible crashworthiness when impact occurs. The thin-walled column and honeycomb core are made of the aluminum alloy AA6060-T4 with density 2.7 × 103 kg/m^3, Young's modulus E = 68.20 GPa, Poisson's ratio = 0.28, initial yielding stress Sy = 80 MPa, ultimate stress Su = 173 MPa and elongation 17.4%. To take strain hardening effects into account, the energy equivalent flow stress can be calculated by using (Wierzbicki 1998)

$$S_0 = \sqrt{\frac{S_y S_u}{1+n}} \tag{22}$$

where n = 0.23 is the strain hardening exponent of the material, and the flow stress for AA6060-T4

Table 2 True stress-plastic strain data points used for mild steel in the numerical simulations

Stress (MPa)	304.6	344.19	385.51	424.88	450.39	470.28
Strain (%)	0	0.0244	0.0485	0.0951	0.1384	0.1910

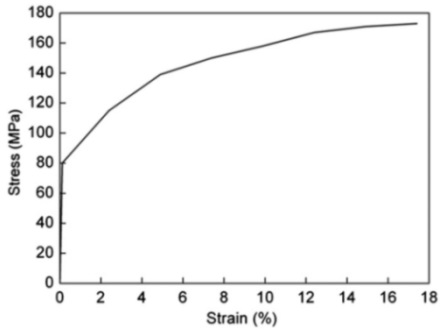

Fig. 5 Tensile stress–strain curve of AA6060-T4

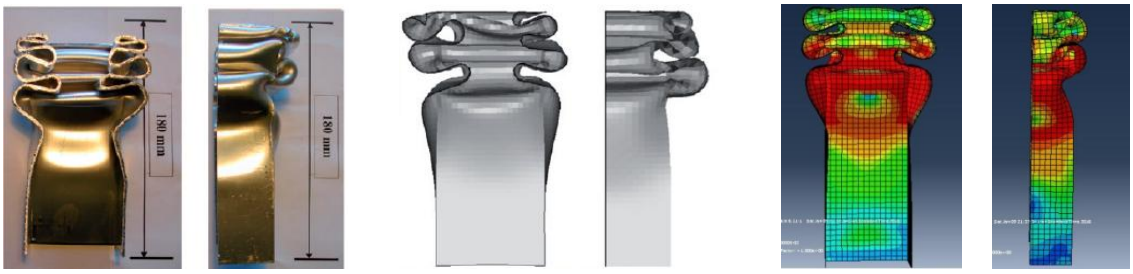

(a) (b) (c)

Fig. 6 Crush pattern of axial impact on tube: (a) experimental dynamic test by Zarei and Kroger; (b) dynamic simulation by Zarei and Krgoer; (c) dynamic simulation in our work

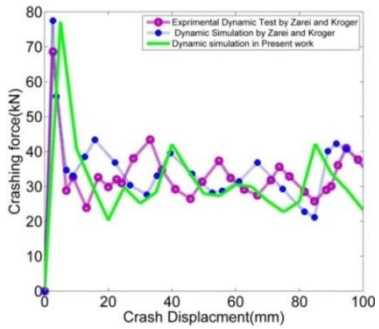

Fig. 7 Crash load-displacement curves of axial impact on tube

adopted here is 106 MPa. The complete stress–strain relation for this material is shown in Fig. 5.

The Diamond core is made of the aluminum alloy. The inner and outer tubes are made of the mild steel for first model and the aluminum alloy for second model. The mild steel considered

with density 7830 kg/m^3, Young's modulus 207 GPa, Poisson's ratio 0.3. The true static stress–strain ratio of the mild steel was obtained using a standard tensile test, from which approximated true stress-plastic strain data points were used in the models, as shown in Table 2.

3. Results and discussion

3.1 RSM Validation results

Crush process of aluminum columns has been experimentally investigated by Zarei and Kroger (2007). Axial impact tests have been conducted on empty aluminum square tubes. The outer diameter of the aluminum tubes is 55 mm, while the wall thickness is 2 mm. Tubes with length of 270 mm are used. Numerical simulations of these crush tests have also been performed in our work to approve the accuracy of the RSM model. Results in Figs. 6 and 7 show that numerical simulation presented in this paper has good agreement with experimental data.

3.2 Finite element and RSM

In order to derive the response functions of SEA and PCF, a series of sampling points (based on K and t) are selected in the design domain to provide sampling designs for FEM. These design points with different K and t values are listed in Table 3. Thus, for each model, 16 honeycomb sandwich columns are obtained resulting in total 32 crash tests. The response functions of SEA and PCF are therefore derived from the finite element analysis results based on the 32 crash tests. After obtaining the FEM results, the required relations of the metamodels based on the RSM can be

Table 3 Design matrix of diamond core sandwich cylindrical columns for crashworthiness

n	Model	K	T (mm)	M (kg)	PCF (kN)	E/M (kJ/kg)	Energy absorption (kJ)
1	Steel tube	1	.5	.64	116.7	6.407	4.101
2		1	1	.79	159.1	6.603	5.217
3		1	1.5	.93	212.9	6.040	5.618
4		1	2	1.08	331.7	9.592	10.36
5		2	.5	.62	105.8	7.904	4.901
6		2	1	.75	129.7	6.981	5.236
7		2	1.5	.87	180.8	6.444	5.607
8		2	2	.99	288	10.444	10.34
9		3	.5	.62	88.45	4.554	2.824
10		3	1	.74	124.7	6.108	4.52
11		3	1.5	.86	183.4	5.015	4.313
12		3	2	.98	228.5	6.236	6.112
13		4	.5	.62	94.12	4.8451	3.004
14		4	1	.73	117.5	4.6726	3.411
15		4	1.5	.85	144.2	4.9047	4.169
16		4	2	.97	207.5	7.659	7.43

Table 3 Continued

n	Model	*K*	*T* (mm)	*M* (kg)	PCF (kN)	E/M (kJ/kg)	Energy absorption (kJ)
1	Aluminum tube	1	.5	.36	62.81	8.522	3.068
2		1	1	.50	87.43	10.802	5.401
3		1	1.5	.65	141.9	13.649	8.872
4		1	2	.79	258.9	17.253	13.63
5		2	.5	.34	67.29	5.205	1.77
6		2	1	.46	91.74	8.141	3.745
7		2	1.5	.59	121.4	6.789	4.006
8		2	2	.93	243	11.924	11.09
9		3	.5	.34	71.47	4.585	1.559
10		3	1	.46	70.87	5.967	2.745
11		3	1.5	.58	99.38	4.834	2.804
12		3	2	.69	133.2	5.834	4.026
13		4	.5	.33	55.67	4.709	1.554
14		4	1	.45	67.49	4.802	2.161
15		4	1.5	.57	92.57	4.405	2.511
16		4	2	.69	128.5	4.636	3.199

Table 4 Accuracies of the metamodels for diamond core sandwich cylindrical columns

Polynomial	Function	Models	RMSE	MAX	R^2	RE%
Linear	SEA (kJ/kg)	Steel tube	1.1863	2.4728	0.4850	[-32.320, 26.384]
		Aluminum tube	1.8168	3.7855	1.8168	[-43.325, 61.994]
	PCF (kN)	Steel tube	21.2378	49.9076	0.9020	[-18.288, 39.076]
		Aluminum tube	28.7222	59.1570	0.7596	[-37.5117, 62.033]
Quadratic	SEA (kJ/kg)	Steel tube	0.9532	1.8307	0.6675	[-31.210,15.832]
		Aluminum tube	0.7699	1.8751	0.9577	[-27.620, 20.034]
	PCF (kN)	Steel tube	8.6932	16.9012	0.9836	[-9.2090,9.2155]
		Aluminum tube	14.6189	35.5613	0.9377	[-27.7362,17.116]
Cubic	SEA (kJ/kg)	Steel tube	0.4736	0.8893	0.9179	[-13.44 , 14.55]
		Aluminum tube	0.5529	1.1150	0.9782	[-16.421, 10.152]
	PCF (kN)	Steel tube	6.6183	16.7312	0.9905	[-5.8404, 9.1228]
		Aluminum tube	9.7982	22.7882	0.9720	[-17.6984, 18.158]
Quartic	SEA (kJ/kg)	Steel tube	16.0359	31.5520	-93.100	[15.304,505.254]
		Aluminum tube	18.0397	35.0785	-22.250	[14.520,756.654]
	PCF (kN)	Steel tube	466.077	925.6016	-46.210	[23.291, 625.106]
		Aluminum tube	310.1477	615.4601	-27.032	[29.2796, 731.858]

developed. As mentioned earlier, the polynomials are usually used as the basis functions in generating these metamodels. In order to find which polynomial best fits the data of Table 3, four different polynomial functions with orders ranging from 1 to 4 (in the form of linear, quadratic, cubic and quartic polynomials) using the results of FEM analysis and based on the RSM are constructed. Then, according to the methodology already described in Section 2.1 for error analysis, the accuracies of these polynomial functions for the honeycomb columns are obtained and summarized in Table 4. From Table 4, it can be found that the cubic polynomial function is the most accurate one in all cases. Thus, the cubic polynomial function is used in RSM models in the following optimization design process.

In order to further validate the RSM method, comparison of the results for sample points is performed by FE simulations. A FE simulation is performed to obtain the values of SEA and PCF in sample points. Then by substituting the sample point values in the cubic polynomial functions of the RSM, the SEA and PCF values are obtained. The results of Table 5 justify the accuracy of the results based on our approach by RSM method.

The response polynomials function of SEA and PCF are

$$PCF_{steel\ tube} = 10^5(1.3575 - 0.5023K + 0.2585t + 0.1012K^2 + 0.2641Kt - 0.0157t^2 - 0.0081K^3 - 0.0055k^2t - 0.1839Kt^2 + 0.2658t^3) \quad (23)$$

$$SEA_{steel\ tube} = 10^4(-0.8348 + 1.7562K + 1.4822t - 0.7793K^2 - 0.0105Kt - 1.5774t^2 + 0.959K^3 + 0.0332k^2t - 0.0654Kt^2 + 0.5367t^3) \quad (24)$$

$$PCF_{\text{Aluminum tube}} = 10^5(-0.6092 + 1.8911K - 0.0372t - 0.8203K^2 + 0.0712Kt + 0.1240t^2 + 0.0995K^3 + 0.0579k^2t - 0.2675t^2 + 0.3107t^3) \quad (25)$$

$$SEA_{\text{Aluminum tube}} = 10^4(0.2466 - 0.2850K + 2.6894t + 0.0266K^2 - 0.2319Kt - 1.8556t^2 + 0.0035K^3 + 0.0350k^2t - 0.0614Kt^2 + 0.5576t^3) \quad (26)$$

The surfaces that were fitted to the SEA and PCF are shown in Figs. 8 and 9. In these figures, the 3D contours of SEA and PCF are plotted to gain more insights into these two models. In each plot, *t* and *K* are set to be in between their minimum and maximum values. It can be seen from the response surface that PCF is increasing as wall thickness *t* and parameter *K* are increasing for the steel and aluminum tube models. However, for aluminum tube it does follow a monotonic pattern.

Table 5 Optimal results obtained using RSM for unconstrained problem

Model	Sample point		RSM result		FEM result		Accuracies RE%	
	K	*T* (mm)	SEA	PCF	SEA	PCF	SEA	PCF
Steel tube	1.83	1.24	7.2268	159.00	7.523	154.5	3.937	-2.912
	2.7	1.58	5.3105	182.217	5.573	189.96	4.710	4.076
Aluminum tube	3.75	1.71	3.8119	95.989	3.694	100.67	-3.191	4.649
	2.25	0.86	6.7703	82.794	6.883	79.924	1.637	-3.590

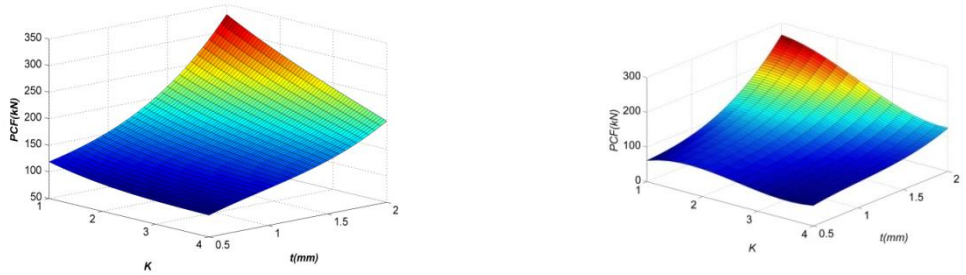

(a) Steel tube (b) Aluminum tube

Fig. 8 The approximate surfaces PCF

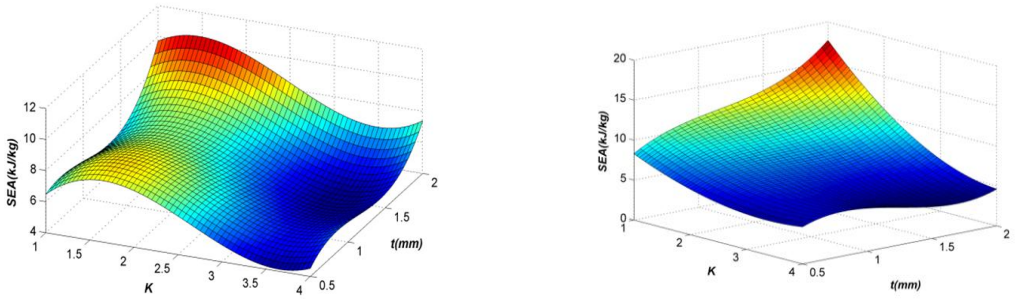

(a) Steel tube (b) Aluminum tube

Fig. 9 The approximate surfaces SEA

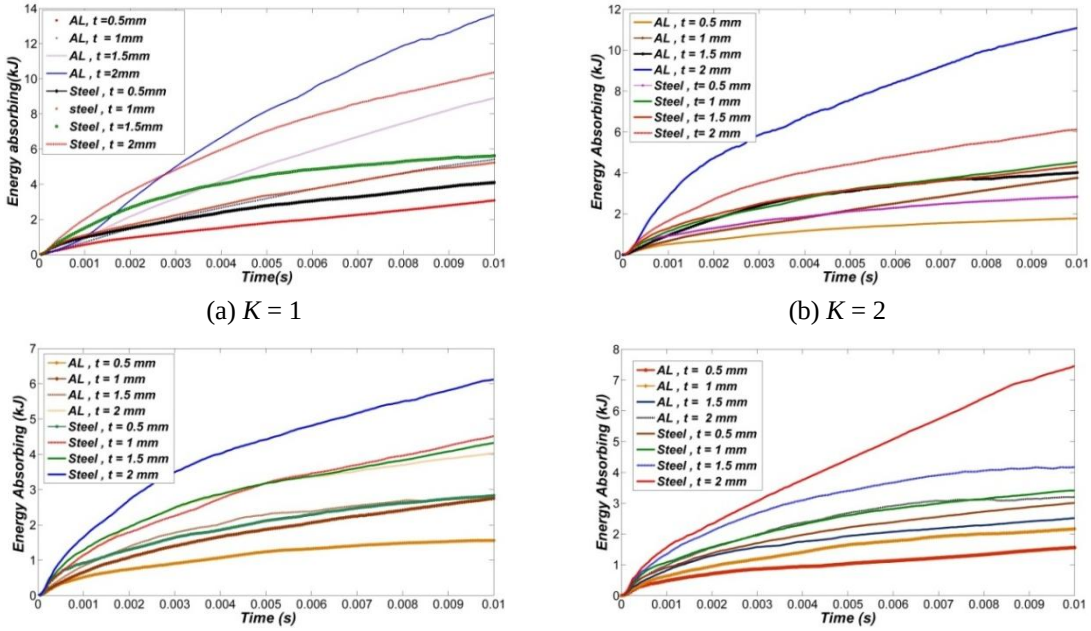

(a) K = 1 (b) K = 2

(c) K = 3 (d) K = 4

Fig. 10 Relationship between mean energy absorbing and honeycomb column thickness vs. time for: (a) K = 1; (b) K = 2; (c) K = 3; (d) K = 4

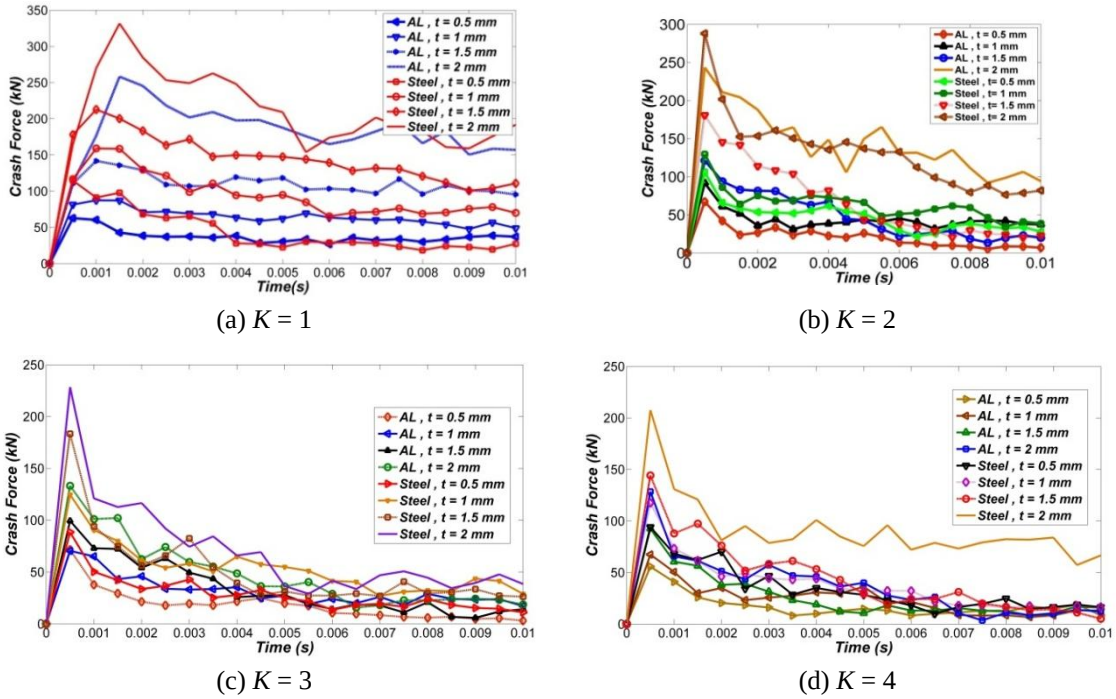

(a) $K = 1$ (b) $K = 2$

(c) $K = 3$ (d) $K = 4$

Fig. 11 Relationship between crushing force and honeycomb column thickness vs. time for: (a) $K = 1$, (b) $K = 2$, (c) $K = 3$, (d) $K = 4$

Honeycomb sandwich columns with two different materials in inner and outer tubs are simulated by FEM. The energy absorption curves obtained from the FEM analysis are also shown in Fig. 10. It is shown that by increasing the honeycomb thickness t, the energy absorption is also increased. Furthermore, the plots show that the energy absorbing for models is decreased by increasing K (Figs. 10(a)-(d)).

The crush force–time curves for two models with different core thickness sizes and K are shown in Fig. 11. During the crushing process, the crush force curve shows a periodic fluctuating behavior which corresponds to the collapse of honeycomb cells. By increasing the wall thickness,

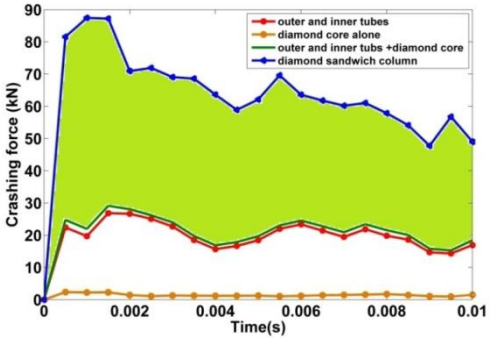

Fig. 12 Crushing force of the diamond core sandwich columns ($t = 1$ mm, $K = 1$, aluminum core)

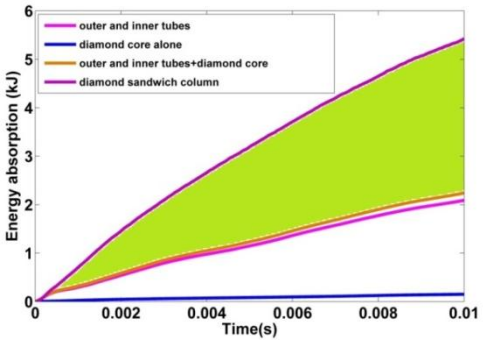

Fig. 13 Energy absorption of the diamond core sandwich columns (t = 1 mm, K = 1, aluminum core)

Table 6 Energy absorption improvement of the honeycomb sandwich columns

E_{core} (J)	E_{tubes} (J)	$E_{core+tubes}$(J)	$E_{sandwich}$(J)	$E_{Improvement}$(J)	% $E_{improvement}$
151.702	2089.74	2241.442	5425.77	3184.328	142.066

PCF is increased. However, by increasing K, the PCF is decreased. Fig. 11 shows that the PCF of the steel model is higher than that of the aluminum tube.

3.3 Interaction effect

The interaction effect between the non-filled bitubal tubes and the core is investigated. Figs. 12 and 13 illustrate the crushing force–time and the energy absorption – time curves for different assemblies of the column including core alone, outer and inner tubes, core plus tubes, and sandwich column, respectively. According to these figures, due to the interaction effect, the level of the crushing force and the energy absorption of the diamond sandwich columns are higher than the summation of the corresponding individual effects of the cores and tubes. The light green area shows clearly the level increase due to the interaction effect.

In Table 6, the energy absorption for the column with core alone, outer and inner tubes, core plus tubes, and sandwich column is given. It can be seen that due to the interaction effect, the energy absorption of the honeycomb sandwich columns is significantly improved when compared to the core plus tubes. This situation is considerable, especially for the aluminum core (t = 1 mm, K = 1) with the improvement about 142%.

3.4 Optimization result

3.4.1 Constrained optimization

With the explicit formulation of SEA (K, t) and PCF (K, t), the constrained single-objective optimization problems is more specifically defined. The optimization problem is defined as

$$\begin{cases} \text{Max.} \quad \text{f} = SEA(K,t) \\ s.t \qquad PCF(K,t) \le 90 \text{ kN} \\ .5 \text{ mm} \le t \le 2 \text{ mm} \\ 1 \le K \le 4 \end{cases} \tag{27}$$

Table 7 Optimal results obtained using RSM models for constrained problem

Model	Optimal point		SEA (kJ/kg) (RSM based)	SEA (kJ/kg) (FEM result)	Accuracies *RE*
	*K**	*t** (mm)			
Steel tube	1.968	0.3010	6.7243	6.5331	-2.926%
Aluminum tube	1.000	1.0979	11.5556	12.1218	4.670%

Table 8 Optimal results obtained using RSM for unconstrained problem

Model	Optimal point		SEA (kJ/kg) (RSM based)	SEA (kJ/kg) (FEM result)	Accuracies *RE*
	*K**	*t** (mm)			
Steel tube	1.4688	2.000	10.4422	9.9213	-5.250%
Aluminum tube	1.000	2.000	17.6987	16.8173	-5.241%

By using the constrained single-objective particle swarm optimization (SOPSO) approach, the optimal results can be obtained as reported in Table 7. From this table, SEA value in the optimal point for aluminum tube is higher than that of the steel tube in the constrained problem. Validation of the optimums is carried out by performing FE simulations. For this purpose, using the optimum values, a FE simulation is performed to obtain the values of SEA. On the other hand, by substituting the optimum values in the cubic polynomial functions of the RSM, another set of the SEA values is obtained. The results of Table 7 show relatively small deviation between the results of RSM and FEM which justifies the accuracy of the results based on our approach.

3.4.2 Unconstrained optimization

To investigate the effect of the PCF constraint on the optimum, an unconstrained optimization problem is also presented herein. In the constrained optimization problem, imposing a constraint on the PCF showed an important role on generating the optimum. By removing the PCF constraint one can obtain different optimal results. The unconstrained optimization is mathematically equivalent to the following problem as

$$\begin{cases} \text{Max.} \quad \text{f} = SEA(K,t) \\ s.t \\ .5 \text{ mm} \le t \le 2 \text{ mm} \\ 1 \le K \le 4 \end{cases} \tag{28}$$

The optimal designs are obtained and given in Table 5. In the optimal point, SEA values for aluminum tube model are higher than that of the steel tube. Validation of the optimums is carried out by performing FE simulations as seen in Table 8 (similar to Table 7).

3.4.3 Multi-objective optimization

In order to design an ideal energy absorber with the highest possible performance, the SEA of the structure must be maximized as an objective function in the crashworthiness optimization problem. On the other hand, it is also very important that the PCF of the structure does not exceed a certain acceptable level. Consequently, minimizing the PCF as another objective function is also much demanded. To consider these two different design criteria, the optimization problem can be written as the following multi-objective optimization forms

$$\begin{cases} \text{Minimize} \quad [PCF(K,t), -SEA(K,t)] \\ \text{subject to} \\ .5 \text{ mm} \le t \le 2 \text{ mm} \\ 1 \le K \le 4 \end{cases} \tag{29}$$

Multi-objective optimization can be formulated in different ways. One of the typical designs account for different criteria in terms of weights to provide different emphasis, as

$$\begin{cases} \text{Minimize} \quad F = w\dfrac{PCF(k,t)}{PCF^*} + (1-w)\dfrac{SEA(k,t)}{SEA^*} \\ \text{subject to} \\ w \in [0,1] \\ .5 \text{ mm} \le t \le 2 \text{ mm} \\ 1 \le K \le 4 \end{cases} \tag{30}$$

where *w* is a weight factor used to adjust the relative importance PCF and SEA to each other, and PCF* and SEA* are the normalization constants for the PCF and SEA, respectively. Here, the values of these normalization constants are taken as the maximum PCF and SEA values obtained at the training points. In this study, the MOPSO algorithm implemented in MATLAB was utilized to generate the Pareto front of the two conflicting objectives of the SEA and PCF. Selection of this optimization algorithm is done due to its relatively low computational cost and fast convergence, as well as the ability to generate the best set of Pareto solutions close to the true Pareto front. PSO is a derivative-free global optimum algorithm and one run could lead to a global optimum. In Table 9, the parameters definition for SOPSO and MOPSO are given.

By using the metamodels and the MOPSO algorithm, the Pareto front of the honeycomb sandwich cylindrical columns under axial crushing loads for the problem is obtained and is shown in Fig. 14. By varying the weight factor *w* in Eq. (30), the Pareto sets for these two models are obtained. In addition, the results of the SOPSO (from Tables 7 and 8) and MOPSO are shown for better comparison. It is clearly observed that the optimums of the SOPSO coincide well with the Pareto points. This implies that the optimal solutions obtained from the SOPSO can be considered as a solution of the MOPSO for the selected SEA and PCF objectives. It is further concluded that the aluminum tube has the best energy absorption capability at a certain peak crushing force.

3.4.4 Application of the multi-criteria decision making method

Having used MOPSO to synthesize a range of solutions, a single solution must be selected by the decision maker. Ranking methods can be used to reduce the non-dominated solution set to a single design. According to the weights reflecting the preference on each objective which is listed in Table 10, TOPSIS is used to rank the non-dominated generated solutions. We can tune up our preference to find the compromise solution that we are satisfied most (Fig. 14). Based on the weights chosen, we finally reach to a specific solution for each design. It is notable that some solutions (designs 2 and 3 of Table 10) distribute in one small region rather than spread over the Pareto space uniformly. It can also be seen that the optimal solution selected by TOPSIS provides a proper compromise between SEA and PCF compared with other Pareto points. To further validate the obtained solutions, we use the corresponding optimal variables *t* and *K* in our crush model to find the SEA and PCF values. Table 10 shows that the simulation results agree well with the MCDM results.

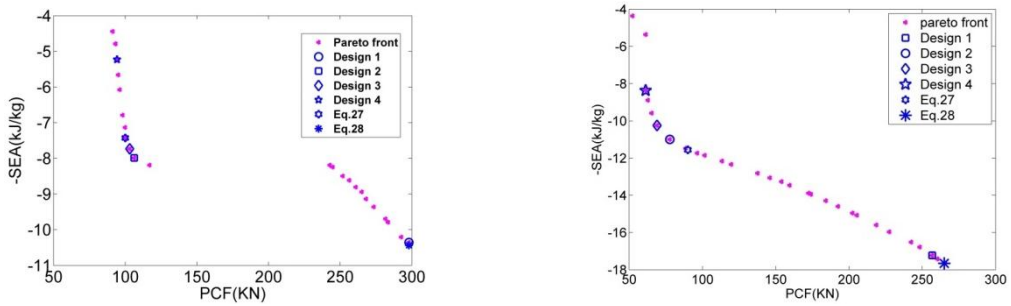

(a) Steel tube (b) Aluminum tube

Fig. 14 Pareto front of – SEA and PCF for the diamond core sandwich column

Table 10 Decision making process, SEA in (kJ/kg) and PCF in (kN)

Model		Weight		MCDM		Simulation	
		SEA	PCF	SEA	PCF	SEA	PCF
Aluminum tube	Design 1	0.75	0.25	17.22	256.68	17.31	260.1
	Design 2	0.5	0.5	11	77.69	10.94	78.35
	Design 3	0.25	0.75	10.25	69.03	10.41	67.74
	Design 4	Entropy method		8.37	61.28	8.43	60.61
Steel tube	Design 1	0.75	0.25	10.35	297.99	10.72	301.43
	Design 2	0.5	0.5	7.98	106.26	7.84	103.98
	Design 3	0.25	0.75	7.73	103.16	7.76	101.12
	Design 4	Entropy method		5.22	94.28	5.19	93.87

Table 9 Parameters definition for PSO optimization

Parameter	MOPSO	SOPSO
Number of particles	100	24
Maximum number of generations	100	100
Self-acceleration constant	0.5	0.5
Social acceleration constant	1	1
Inertia constant	0.8	0.7
Velocity band	1.3	1

3.5 Sensitivity results

3.5.1 Local sensitivity

In this section, we investigate the sensitivity of SEA and PCF with respect to the design variables *K* and *t*. Fig. 15 shows the normalized local sensitivity measures of SEA and PCF for the design domain. The sensitivity measure with respect to each variable is illustrated in the form of a surface. As it can clearly be observed for aluminum tube, in the majority of the design domain, the SEA is more sensitive to the variations of *t* compared to *K* as the corresponding sensitivity surface

of *t* is above the other surface. This implies that variations of *t* show greater influence on the variations of SEA compared to the variations of *K*. The points located on the intersection of two sensitivity surfaces represent regions of the design domain for which the sensitivity of the SEA is equal with respect to both *K* and *t*. From Figs. 15(b), (c), sensitivity surfaces have two intersection curves while for Fig. 15(d), only one intersection curve is obtained.

3.5.2 Global sensitivity analysis

The trial function was calculated and the sensitivity measures considering first order and total effects of the parameters are obtained and shown in Table 11. From the presented results, it is seen that the design variable *K* has greater effect on the sensitivity of SEA functions for two models. Also, the design variable *t* has greater effect on the sensitivity of PCF functions for two models.

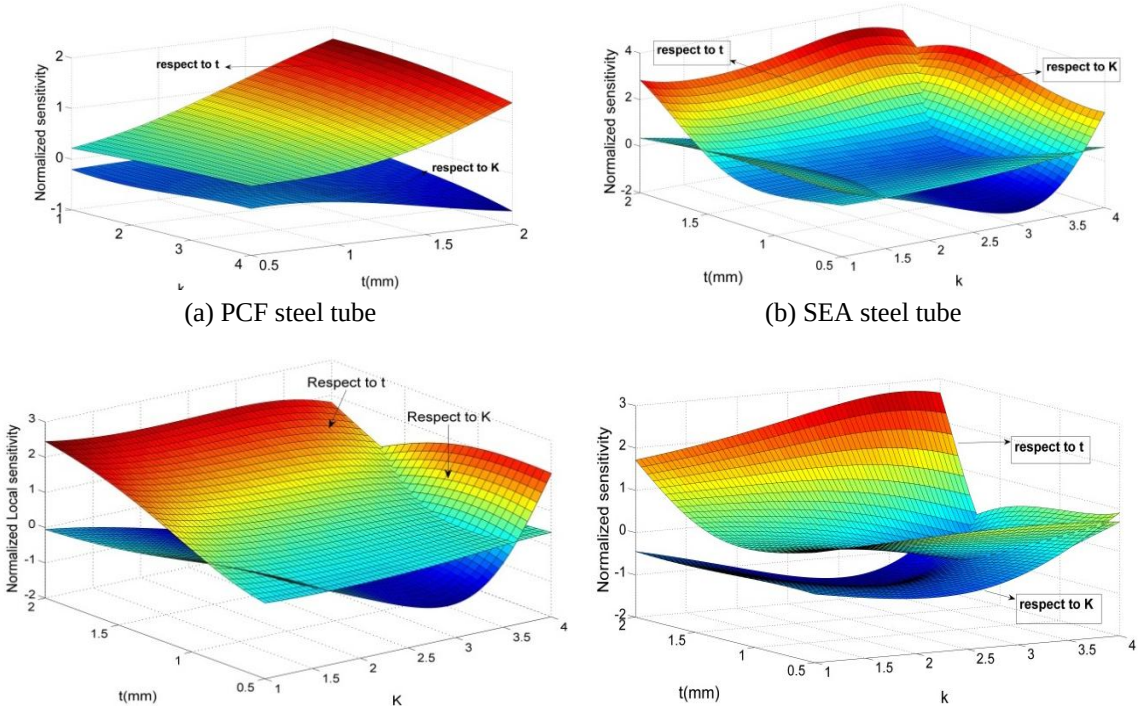

(a) PCF steel tube (b) SEA steel tube

(c) PCF aluminum tube (d) SEA aluminum tube

Fig. 15 Normalized sensitivity for SEA and PCF

Table 11 Sobol's method of sensitivity analysis

Function	Models	First order effects		Total effects	
		Respect to K	Respect to t	Respect to K	Respect to t
SEA(kJ/kg)	Steel tube	0.8123	0.1744	0.8256	0.1877
	Aluminum tube	0.8307	0.0707	0.9293	0.1693
PCF(kN)	Steel tube	0.1185	0.8593	0.1407	0.8815
	Aluminum tube	0.2389	0.6679	0.3321	0.7611

By considering the first order and total effects, the sensitivity measure of the SEA with respect to *K* has its higher values for the aluminum tube. In addition, with respect the first order and total effects, the sensitivity measures of the PCF with respect to *t* is higher for the steel tube model.

4. Conclusions

This paper studied the single-objective and multi-objective optimizations of diamond core honeycomb sandwich cylindrical columns for two models by nonlinear finite element analysis under axial crushing loads. These two models differed in materials of inner or outer tubes that contain steel or aluminum. After validation of the RSM approach and the dynamic model, a multi-objective problem was formulated to maximize the SEA and minimize the PCF with respect to the pitch of honeycomb core *K* and core thickness *t*. The MOPSO algorithm was applied to generate the Pareto fronts for different multi-objective problems using the metamodels constructed from the RSM and FEM results. The constrained single-objective particle swarm optimization (SOPSO) was applied to find the optimal design variables for each model by maximizing the SEA for a certain PCF as constraint. Optimization results showed that the energy absorption characteristics with constrained and unconstrained peak crashing load were improved. Also, it was concluded that the aluminum tube has a better energy absorption capability compared to the steel tube at a certain peak crushing force. The results justified that the interaction effects between the honeycomb and column walls greatly improve the energy absorption efficiency.

Furthermore, the TOPSIS method was used for solving MCDM problem. According to the weights reflecting the preference on each objective, TOPSIS was used to rank the non-dominated solutions generated. It was notable that some solutions distributed in one small region rather than spread over the Pareto space uniformly. It could also be seen that the optimal solution selected by TOPSIS provided a proper compromise between SEA and PCF compared with other Pareto points.

Finally, based on a normalized local sensitivity analysis of aluminum tube, it was observed that in the majority of the design domain, the SEA is more sensitive to the variations of *t* compared to *K*. This implies that variations of the design variable *t* show greater influence on the variations of SEA compared to the variations of *K*. From the global sensitivity results, it was seen that the design variable *K* has greater effect on the sensitivity of SEA for two models. Also, the design variable *t* has greater effect on the sensitivity of PCF functions for two models.

References

Abramowicz, W. and Jones, N. (1984a), "Dynamic axial crushing of square tubes", *Int. J. Impact Eng.*, **2**(2), 179-208.

Abramowicz, W. and Jones, N. (1984b), "Dynamic axial crushing of circular tubes", *Int. J. Impact Eng.*, **2**(3), 263-281.

Acar, E., Guler, M.A., Gerçeker, B., Cerit, M.E. and Bayram, B. (2011), "Multi-objective crashworthiness optimization of tapered thin-walled tubes with axisymmetric indentations", *Thin-Wall. Struct.*, **49**(1), 94-105.

Athan, T.W. and Papalambros, P.Y. (1999), "A note on weighted criteria methods for compromise solutions in multi-objective optimization", *Eng. Optim.*, **27**(2), 155-176.

Avalle, M., Chiandussi, G. and Belingardi, G. (2002), "Design optimization by response surface methodology: application to crashworthiness design of vehicle structures", *Struct. Multidiscip. Optim.*, **24**(4), 325-332.

Chen, M.F. and Tzeng, G.H. (2004), "Combining grey relation and TOPSIS concepts for selecting an expatriate host country", *Math. Comput. Model*, **40**(13), 1473-1490.
Chiandussi, G. and Avalle, M. (2002), "Maximization of the crushing performance of a tubular device by shape optimization", *Comput. Struct.*, **80**(27-30), 2425-2432.
Deng, H., Yeh, C.H. and Willis, R.J. (2000), "Inter-company comparison using modified TOPSIS with objective weights", *Comput. Operat. Res.*, **27**(10), 963-973.
Ebrahimi, S. and Vahdatazad, N. (2015), "Multi-objective optimization and sensitivity analysis of honeycomb sandwich cylindrical columns under axial crushing loads", *Thin-Wall. Struct.*, **88**, 90-104.
Fang, H., Rais-Rohani, M., Liu, Z. and Horstemeyer, M.F. (2005), "A comparative study of metamodeling methods for multi-objective crashworthiness optimization", *Comput. Struct.*, **83**(25-26), 2121-2136.
Fang, J., Gao, Y., Sun, G., Xu, C. and Li, Q. (2015), "Multi objective robust design optimization of fatigue life for a truck cab", *Reliab. Eng. Syst. Safe.*, **135**, 1-8.
Forsberg, J. and Nilsson, L. (2005), "On polynomial response surfaces and Kriging for use in structural optimization of crashworthiness", *Struct. Multidiscip. Optim.*, **29**(3), 232-243.
Forsberg, J. and Nilsson, L. (2006), "Evaluation of response surface methodologies used in crashworthiness optimization", *Int. J. Impact Eng.*, **32**(5), 759-777.
Hou, S.J., Li, Q., Long, S.Y., Yang, X.J. and Li, W. (2007), "Design optimization of regular hexagonal thin walled columns with crashworthiness criteria", *Finite Elem. Anal. Des.*, **43**(6-7), 555-565.
Hou, S.J., Li, Q., Long, S.Y., Yang, X.J. and Li, W. (2008), "Multi-objective optimization of multi-cell sections for the crashworthiness design", *Int. J. Impact Eng.*, **35**(11), 1355-1367.
Hou, S., Li, Q., Long, S., Yang, X. and Li, W. (2009), "Crashworthiness design for foam filled thin-wall structures", *Mater. Des.*, **30**(6), 2024-2032.
Hwang, C.L. and Yoon, K. (1981), *Multiple Attribute Decision Making*: *Methods and Applications*, Berlin/Heidelberg/New York, Springer-Verlag.
Jansson, T., Nilsson, L. and Redhe, M. (2003), "Using surrogate models and response surface in structural optimization with application to crashworthiness design and sheet metal forming", *Struct Multidiscip. Optim.*, **25**(2), 129-140.
Kennedy, J. and Eberhart, R.C. (1995), "Particle swarm optimization", *Proceedings of the IEEE International Joint Conference on Neural Networks*, Piscataway, NJ, USA, November-December, pp. 1942-1948.
Kim, H.S. (2002), "New extruded multi cell aluminum profile for maximum crush energy absorption and weight efficiency", *Thin-Wall. Struct.*, **40**(4), 311-327.
Kodiyalam, S., Yang, R.J., Gu, L. and Tho, C.H. (2004), "Multidisciplinary design optimization of a vehicle system in a scalable, high performance computing environment", *Struct. Multidiscip. Optim.*, **26**(3), 256-263.
Lanzi, L., Castelletti, M.L. and Anghileri, M. (2004), "Multi-objective optimization of composite absorber shape under crashworthiness requirements", *Compos. Struct.*, **65**(3-4), 433-441.
Lee, T.H. and Lee, K. (2005), "Multi-criteria shape optimization of a funnel in cathode ray tubes using a response surface model", *Struct. Multidiscip. Optim.*, **29**(5), 374-381.
Lee, S.H., Kim, H.Y. and Oh, I.S. (2002), "Cylindrical tube optimization using response surface method based on stochastic process", *J. Mater. Process. Technol.*, **130-131**, 490-496.
Li, M., Deng, Z., Guo, H., Liu, R. and Ding, B. (2014), "Optimizing crashworthiness design of square honeycomb structure", *J. Cent. South Univ.*, **21**(3), 912-919.
Liao, X.T., Li, Q., Yang, X.J., Zhang, W.G. and Li, W. (2007), "Multiobjective optimization for crash safety design of vehicles using stepwise regression model", *Struct. Multidiscip. Optim*, **35**(6), 561-569. DOI: 10.1007/s00158-007-0163-x
Lin, C.T., Chang, C.W. and Chen, C.B. (2006), "The worst ill-conditioned silicon wafer slicing machine detected by using Grey relational analysis", *Int. J. Adv. Manuf. Technol.*, **31**(3), 388-395.
Lu, G. and Yu, T. (2003), *Energy Absorption of Structures and Materials*, Wood Head Publishing Ltd., Cambridge, England.
Myers, R.H. and Montgomery, D.C. (2002), *Response Surface Methodology*, Wiley, New York, NY, USA.

Oktem, H., Erzurumlu, T. and Kurtaran, H. (2005), "Application of response surface methodology in the optimization of cutting conditions for surface roughness", *J. Mater. Process. Technol.*, **170**(1-2), 11-16.
Saltelli, A., Ratto, M., Tarantola, S. and Campolongo, F. (2006), "Sensitivity analysis practices: Strategies for model-based inference", *Reliab. Eng. Syst. Safe.*, **91**(10-11), 1109-1125.
Saltelli, A., Ratto, M., Andres, T., Campolongo, F., Cariboni, J., Gatelli, D., Saisana, M. and Tarantola, S. (2008), *Global Sensitivity Analysis*, The Primer, John Wiley & Sons.
Sinha, K. (2007), "Reliability-based multi-objective optimization for automotive crashworthiness and occupant safety", *Struct. Multidiscip. Optim.*, **33**(3), 255-268.
Sun, G., Li, G., Stone, M. and Li, Q. (2010a), "A two-stage multi-fidelity optimization procedure for honeycomb-type cellular materials", *Compos. Mater. Sci.*, **49**(3), 500-511.
Sun, G., Li, G., Hou, S., Zhou, S., Li, W. and Li, Q. (2010b), "Crashworthiness design for functionally graded foam-filled thin-walled structures", *Mater. Sci. Eng. A-Struct.*, **527**(7-8), 1911-1919.
Sun, G., Song, X., Baek, S. and Li, Q. (2014), "Robust optimization of foam-filled thin-walled structure based on sequential Kriging metamodel", *Struct. Multidiscip. Optim.*, **49**(6), 897-913
Wang, G.G. and Shan, S. (2007), "Review of metamodeling techniques in support of engineering design optimization", *J. Mech. Des.*, **129**(4), 370-380.
Wierzbicki, T. (1998), "Crash behavior of box columns filled with aluminum honeycomb or foam", *Compos. Struct.*, **68**(4), 343-367.
Xiang, Y.J., Wang, Q., Fan, Z.J. and Fang, H.B. (2006), "Optimal crashworthiness design of a spot-welded thin-walled hat section", *Finite Elem. Anal. Des.*, **42**(10), 846-855.
Yang, R.J., Wang, N., Tho, C.H., Bobineau, J.P. and Wang, B.P. (2005), "Metamodeling development for vehicle frontal impact simulation", *J. Mech. Des.*, **127**(5), 1014-1020.
Yin, H., Wen, G., Hou, S. and Chen, K. (2011), "Crushing analysis and multi-objective crashworthiness optimization of honeycomb-filled single and bitubular polygonal tubes", *Mater. Des.*, **32**, 4449-4460.
Yin, H., Wen, G., Liu, Z. and Qing, Q. (2014), "Crashworthiness optimization design for foam-filled multi-cell thin-walled structures", *Thin-Wall. Struct.*, **75**, 8-17.
Zarei, H.R. and Kroger, M. (2006), "Multi-objective crashworthiness optimization of circular aluminum tubes", *Thin-Wall. Struct.*, **44**(3), 301-308.
Zarei, H.R. and Kroger, M. (2007), "Optimum honeycomb filled crash absorber design", *Mater. Des.*, **29**(1), 193-204.
Zhang, Z., Liu, S. and Tang, Z. (2010), "Crushworthiness investigation of kagome honeycomb sandwich cylindrical column under axial crushing loads", *Thin-Wall. Struct.*, **48**(1), 9-18.
Zhang, Z., Liu, S. and Tang, Z. (2011), "Comparisons of honeycomb sandwich and foam-filled cylindrical columns under axial crushing loads", *Thin-Wall. Struct.*, **49**(9), 1071-1079.

CC